Dielectronic satellite contributions to Ne VIII and Ne IX *K*-shell spectra

B. J. Wargelin* and S. M. Kahn†
Department of Physics and Space Sciences Laboratory, University of California, Berkeley, California 94720

P. Beiersdorfer
Lawrence Livermore National Laboratory, 7000 East Avenue, Livermore, California 94550

(Received 8 August 2000; published 17 January 2001)

$K\alpha$ spectra of heliumlike neon and associated lithiumlike, berylliumlike, and boronlike satellite line emission have been observed with a high-resolution crystal spectrometer on the Lawrence Livermore Electron Beam Ion Trap. The *KLL* dielectronic recombination satellites were resolved from their He-like parent lines in electron energy space, and their wavelengths and resonance strengths measured. The wavelength measurements achieved a typical accuracy of a few mÅ, with two measurements accurate to better than one part in 10 000. By normalizing to the He-like resonance line, *w*, we measure Li-like satellite resonance strengths that are 10% to 46% lower than predicted by theoretical models. The wavelengths and relative strengths of Be-like *KLL* satellites were also measured, and absolute strengths were obtained by normalizing to the collisionally excited Li-like *qr* satellite blend.

DOI: 10.1103/PhysRevA.63.022710 PACS number(s): 32.80.Hd, 32.30.Rj, 32.70.Fw, 34.80.Kw

I. INTRODUCTION

In addition to its role in determining a plasma's charge balance, dielectronic recombination (DR) is important in x-ray emitting astrophysical and laboratory plasmas because of the resulting satellite emission lines. These satellites often blend with their parent emission lines or lines from other ions, thus affecting those lines' apparent intensities. Likewise, the closely related process of resonant excitation can lead to enhanced emission of the primary emission lines themselves. These resonance phenomena are particularly important for He-like ions, whose $K\alpha$ lines have several diagnostic uses, including the determination of electron density, temperature, and element abundance. The relative intensities of the satellites can also, when resolvable, provide information on the electron temperature, or deviations from a Maxwellian energy distribution.

From an astrophysical point of view, the He-like neon spectrum is particularly rewarding to study because of its electron density diagnostic, which is most sensitive at roughly 10^{12} cm^{-3}. This is just above the typical density of stellar coronae ($\sim 10^{10}$ cm^{-3}), and a good match for the densities in stellar flares, which can range up to several times 10^{13} cm^{-3}. The He-like neon spectrum is, however, challenging to study because it overlaps with the ubiquitous iron *L*-shell emission. Even in the high-resolution spectra obtained with the *Chandra* and *XMM-Newton* x-ray observatories, great care must be used to determine the contributions of individual lines. This requires accurate knowledge of line wavelengths and the relative intensities of primary emission lines and their satellites.

Much of the confusion associated with line blending can be alleviated by using an electron beam ion trap (EBIT), which allows study of collisional emission spectra as a function of wavelength *and* electron collision energy. Measurements are therefore level-specific, permitting the determination of the wavelength, excitation energy, and strength of individual resonances. The degree of completeness and detail available in such measurements often exceeds that provided in theoretical studies, which may not list all the relevant autoionization and radiative rates needed for proper comparison. Indeed, published results usually integrate over all energies and sum individual satellites together.

This paper presents results from an EBIT study of the lowest-energy DR resonances in He-like, Li-like, and Be-like neon, and is part of a larger program to experimentally characterize $K\alpha$ line emission from heliumlike neon as completely as possible. Measurements of the radiative lifetime of the metastable $1s2s\,^3S_1$ level, the basis of the important density diagnostic, have already been reported [1,2]. Future papers will present results on the measured cross sections for collisional transfer from the metastable level, resonant excitation and near-threshold DR, inner-shell ionization of Li-like Ne (which populates the He-like metastable level), and direct electron impact excitation.

II. THEORY

A. Overview of He-like $K\alpha$ lines and their satellites

As shown in Fig. 1, there are six levels in the He-like $1s2l$ configuration, four of which have single-photon radiative decays of the form

$$1s2l \rightarrow 1s^2 + h\nu, \tag{1}$$

giving rise to the so-called *resonance* line *w* ($1s2p\,^1P_1 \rightarrow 1s^2\,^1S_0$), *intercombination* lines *x* and *y* ($1s2p\,^3P_{2,1} \rightarrow 1s^2\,^1S_0$), and *forbidden* line *z* ($1s2s\,^3S_1 \rightarrow 1s^2\,^1S_0$), where we have used the *w*,*x*,*y*,*z* notation of Gabriel [3].

*Present address: Harvard-Smithsonian Center for Astrophysics, 60 Garden Street, Cambridge, MA 02138.

†Present address: Department of Physics, Columbia University, 538 West 120th Street, New York, NY 10027.

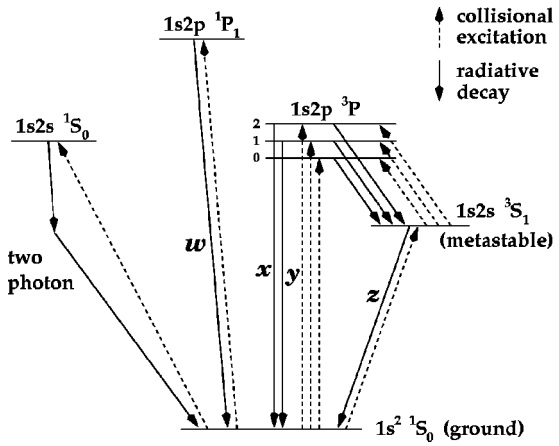

FIG. 1. Energy-level diagram showing ground state and first excited states ($1s2l$) of a He-like ion. Line *w* is the resonance line, *x* and *y* are the intercombination lines, and *z* is the forbidden line. Energy differences are not to scale; all excited states are much closer to each other than to the ground state. Satellite lines have essentially the same transitions but with one or more spectator electrons.

Satellite lines are produced when at least one extra spectator electron is present, in transitions of the form

$$1s2ln'l' \rightarrow 1s^2n'l' + h\nu'. \tag{2}$$

The spectator $n'l'$ electron partially shields the nuclear charge, so that satellite lines are slightly shifted toward longer wavelengths relative to their parent lines. The shift is largest for $n'=2$ spectator electrons and approaches zero as $n' \rightarrow \infty$. Satellite intensity decreases with increasing n'; this paper addresses only the strongest, $2l'$ satellites.

There are 16 levels in the Li-like $1s2l2l'$ configuration, with 22 dipole-allowed $2 \rightarrow 1$ transitions to the three Li-like $1s^22l$ ''ground'' levels. Gabriel [3] labels these satellite lines with the letters *a* through *v*. Similarly, there are 30 levels of the type $1s2l(2l')^2$ in Be-like ions and 35 $1s2l(2l')^3$ levels in B-like, which can, respectively, decay to 10 and 15 ground levels, producing a total of 102 and 217 dipole-allowed $\Delta n=1$ satellite transitions. Only a fraction of these lines are strong enough to be observed, and the main satellites in Li-like, Be-like, and B-like neon are grouped around three or four wavelengths for each ion.

Multiply excited states such as those described above can either (i) emit a satellite line via a radiatively stabilizing transition to a bound (nonautoionizing) state, or (ii) autoionize (undergo Auger emission), in which one of the excited electrons falls to a lower-energy subshell while another excited electron carries away the energy of that transition by being ejected into the continuum. The net emission cross section for a satellite line is therefore equal to the cross section for excitation of the state that emits the line times the fluorescence yield, *W*, which is the probability that the state decays radiatively and emits the line. For excitation of a satellite line *s* from an initial state $|i\rangle$ which at low densities is virtually always the ground state, to an intermediate autoionizing state $|s\rangle$ and then to a final state $|f\rangle$ by radiative decay, this net cross section can be written as

$$\sigma_s(E) = \sigma_{is}(E) W_{sf}, \tag{3}$$

where *E* is the energy of the colliding electron.

Several transitions may be possible from an excited state. The fluorescence yield for a particular satellite line is given by

$$W_s = \frac{A_{sf}^{\mathrm{rad}}}{\sum_j A_{sj}^{\mathrm{auto}} + \sum_k A_{sk}^{\mathrm{rad}}}, \tag{4}$$

where A_{sf}^{rad} is the rate (in sec^{-1}) for radiative decay from state $|s\rangle$ to state $|f\rangle$, the second summed term in the denominator represents the total rate of radiative decay from state $|s\rangle$, and the first sum extends over all levels which are populated by autoionization of level $|s\rangle$ (for instance, a $1s2lnl'$ state autoionizes to $1s^2$, while a $1s3lnl'$ state can autoionize to $1s2l$ or $1s^2$). Note that for singly excited (nonautoionizing) states, the fluorescence yield simply reduces to a radiative branching ratio.

B. Dielectronic recombination

There are three ways to excite an autoionizing state via electron collisions: inner-shell ionization, inner-shell excitation, and dielectronic recombination (DR). Each of these processes tends to favor the production of a different set of autoionizing states, although individual states can often be excited in more than one way. Inner-shell ionization of a Be-like ion creates an autoionizing Li-like ion ($1s2s^2$), and ionization of a B-like ion leaves a Be-like ion ($1s2s^22p$). The fluorescence yields from those excited configurations, however, are very low and satellite emission is negligible. Inner-shell ionization of Li-like ions, in contrast, often leads to the emission of the He-like forbidden line, *z*.

Likewise, innershell excitation of a Li-like ion to a $1s2sn'l'$ level, particularly in the $1s2s2p$ configuration, produces significant satellite line emission, primarily from the *q* and *r* blend (see Table I), which has a combined excitation cross section nearly as large as that of the He-like parent line, *w*. This direct collisional excitation occurs only above a threshold energy, which is slightly below that necessary for excitation of the parent He-like line due to the shielding effect of the $n'=2$ electron. Satellites can also be produced when the colliding electron has an energy *below* the direct excitation threshold via dielectronic recombination.

The first step in the DR process is dielectronic capture, which is like radiative recombination except that instead of carrying away the recombination energy via a photon, one of the initially bound electrons is excited to a higher-energy level. Since these energy levels are quantized, this is a resonant process, i.e., it can only occur at discrete energies. DR resonances are usually labeled using the notation for the inverse autoionization process, e.g., *KLM* denotes the DR resonance in which a *K*-shell electron is excited to the *L* shell by the capture of a continuum electron into the *M* shell. After dielectronic capture, the ion is left in a multiply excited state which will, as explained earlier, either decay radiatively to a

TABLE I. Theoretical atomic data for KLL dielectronic satellite transitions $1s2l2l' \rightarrow 1s^2 2l'$ in Li-like Ne^{7+}. Transitions are labeled as by Gabriel [3] using LS coupling notation, and with j marked for the p electrons of the upper level, as given by Nilsen [19]. E_{res} is the resonance energy, using the average of the values of Chen [12] and Karim and Bhalla [13], which agree to within 1.3 eV for all lines. P is the line polarization and G_s/G_w is the spectrometer response function for line s relative to that for w. S is the transition strength, in units of 10^{-20} cm^2 eV; negative numbers in brackets indicate powers of 10.

Line	Transition	E_{res}	P [a]	G_s/G_w	λ [b] (Å)	λ [c] (Å)	λ [d] (Å)	λ [e] (Å)	S [b]	S [c]	S [d]	S [e]
a	$1s2p_{3/2}^2\ ^2P_{3/2} \rightarrow 1s^2 2p\ ^2P_{3/2}$	683.70	−0.75	0.387	13.675	13.6755	13.6995	13.6702	0.652	0.384	0.452	0.583
b	$1s2p_{3/2}^2\ ^2P_{3/2} \rightarrow 1s^2 2p\ ^2P_{1/2}$	683.70	+0.60	0.939	13.672	13.6724	13.6967	13.6667	0.110	0.065	0.076	0.144
c	$1s2p_{1/2}2p_{3/2}\ ^2P_{1/2} \rightarrow 1s^2 2p\ ^2P_{3/2}$	683.50	0	0.632	13.678	13.6785	13.7026	13.6732	7.5[−4]	2.5[−3]	9.2[−4]	2.8[−4]
d	$1s2p_{1/2}2p_{3/2}\ ^2P_{1/2} \rightarrow 1s^2 2p\ ^2P_{1/2}$	683.50	0	0.632	13.675	13.6755	13.6998	13.6697	1.6[−3]	5.2[−3]	1.9[−3]	5.7[−4]
e	$1s2p_{3/2}^2\ ^4P_{5/2} \rightarrow 1s^2 2p\ ^2P_{3/2}$	673.88	0.50	0.867	13.819	13.8332	13.8557	13.8187	3.6[−3]	2.3[−3]	2.8[−3]	2.1[−3]
f	$1s2p_{1/2}2p_{3/2}\ ^4P_{3/2} \rightarrow 1s^2 2p\ ^2P_{3/2}$	673.52	−0.75	0.379	13.820	13.8347	13.8573	13.8211	1.4[−3]	2.0[−4]	1.0[−3]	2.6[−4]
g	$1s2p_{1/2}2p_{3/2}\ ^4P_{3/2} \rightarrow 1s^2 2p\ ^2P_{1/2}$	673.52	+0.60	0.928		13.8316		13.8175		5.6[−6]		4.5[−4]
h	$1s2p_{1/2}^2\ ^4P_{1/2} \rightarrow 1s^2 2p\ ^2P_{3/2}$	673.43	0	0.623		13.8363		13.8226		2.0[−8]		9.4[−8]
i	$1s2p_{1/2}^2\ ^4P_{1/2} \rightarrow 1s^2 2p\ ^2P_{1/2}$	673.43	0	0.623	13.819	13.8332	13.8559	13.8190	1.6[−4]	5.1[−7]	1.7[−4]	2.1[−6]
j	$1s2p_{1/2}2p_{3/2}\ ^2D_{5/2} \rightarrow 1s^2 2p\ ^2P_{3/2}$	681.95	+0.50	0.875	13.711	13.7104	13.7344	13.6969	8.783	7.295	8.674	7.643
k	$1s2p_{1/2}2p_{3/2}\ ^2D_{3/2} \rightarrow 1s^2 2p\ ^2P_{1/2}$	681.97	+0.60	0.936	13.707	13.7062	13.7305	13.6936	5.299	4.391	5.226	3.782
l	$1s2p_{1/2}2p_{3/2}\ ^2D_{3/2} \rightarrow 1s^2 2p\ ^2P_{3/2}$	681.97	−0.75	0.385	13.710	13.7093	13.7333	13.6971	0.610	0.494	0.584	1.366
m	$1s2p_{3/2}^2\ ^2S_{1/2} \rightarrow 1s^2 2p\ ^2P_{3/2}$	693.84	0	0.639	13.539	13.5293	13.5500	13.5225	1.584	1.395	1.538	1.298
n	$1s2p_{3/2}^2\ ^2S_{1/2} \rightarrow 1s^2 2p\ ^2P_{1/2}$	693.84	0	0.639	13.536	13.5263	13.5473	13.5190	0.699	0.621	0.689	0.579
o	$1s2s^2\ ^2S_{1/2} \rightarrow 1s^2 2p\ ^2P_{3/2}$	651.40	0	0.595	14.163	14.1842	14.1956	14.1692	0.189	0.168	0.234	0.174
p	$1s2s^2\ ^2S_{1/2} \rightarrow 1s^2 2p\ ^2P_{1/2}$	651.40	0	0.596	14.160	14.1809	14.1926	14.1654	0.098	0.087	0.121	0.090
q	$1s(2s2p_{3/2}\ ^3P)^2 P_{3/2} \rightarrow 1s^2 2s^2 S_{1/2}$	667.99	+0.60	0.936	13.652	13.6681	13.6759	13.6551	4.073	5.887	5.591	4.576
r	$1s(2s2p_{3/2}\ ^3P)^2 P_{1/2} \rightarrow 1s^2 2s^2 S_{1/2}$	667.84	0	0.633	13.654	13.6705	13.6779	13.6571	2.455	3.074	3.070	2.470
s	$1s(2s2p_{3/2}\ ^1P)^2 P_{3/2} \rightarrow 1s^2 2s\ ^2S_{1/2}$	675.62	+0.60	0.942	13.564	13.5655	13.5796	13.5452	1.025	1.351	1.095	1.205
t	$1s(2s2p_{3/2}\ ^1P)^2 P_{1/2} \rightarrow 1s^2 2s^2 S_{1/2}$	675.59	0	0.638	13.565	13.5655	13.5800	13.5461	0.637	0.773	0.663	0.692
u	$1s2s2p_{1/2}\ ^4P_{3/2} \rightarrow 1s^2 2s^2 S_{1/2}$	655.99	+0.60	0.922	13.835	13.8537	13.8692	13.8356	9.0[−4]	3.7[−4]	7.2[−4]	5.4[−4]
v	$1s2s2p_{1/2}\ ^4P_{1/2} \rightarrow 1s^2 2s^2 S_{1/2}$	655.92	0	0.622	13.836	13.8544	13.8699	13.8371	2.4[−4]	2.4[−4]	8.0[−5]	1.1[−4]

[a] Inal and Dubau [9].
[b] Vainshtein and Safronova [8].
[c] Chen [12].
[d] Nilsen [19].
[e] Karim and Bhalla [13].

singly excited state, resulting in dielectronic recombination and the retention of the additional electron, or autoionize, resulting in either resonant excitation or resonant elastic scattering.

Cross sections for a resonant process such as DR are of course extremely energy-dependent, with Lorentzian shapes and natural widths of less than 1 eV. For satellite lines excited by DR, it is therefore more useful to speak of an *integrated* cross section, or resonance strength. If we define the satellite resonance strength S_s as the integral over all energies of cross section $\sigma_s(E)$ for emission of line s via the process $|i\rangle \rightarrow |s\rangle \rightarrow |f\rangle$, then Eq. (3) becomes

$$S_s = \int_0^\infty \sigma_s(E)dE = \int_0^\infty \sigma_{is}(E)W_s dE = S_{is}W_s . \qquad (5)$$

This simply states that the satellite resonance strength is equal to the dielectronic capture resonance strength, S_{is}, times the fluorescence yield.

Because dielectronic capture is the inverse of autoionization, S_{is} is proportional to $A_{si}^{\rm auto}$ by the principle of detailed balance. The full equation is

$$S_{is} = \frac{\pi^2}{k_i^2}\frac{g_s}{g_i}A_{si}^{\rm auto} = \frac{2\pi^2 a_0^3 \mathcal{R}^2}{E_{\rm res}}\sqrt{\frac{m_e}{2R_y}}\frac{g_s}{g_i}A_{si}^{\rm auto}, \qquad (6)$$

where k_i is the electron wave number corresponding to the resonance energy, g_s is the statistical weight of the autoionizing level (equal to $2J_s+1$), g_i is the weight of the initial level (equal to 1 for the He-like ground state, 2 for Li-like), a_0 is the Bohr radius, $\mathcal{R}$ is the Rydberg energy, and m_e is the electron mass. It is common to refer to a satellite intensity factor, defined as

$$Q_s = g_s A_{si}^{\rm auto} W_s = \frac{g_s A_{si}^{\rm auto} A_{sf}^{\rm rad}}{\sum_j A_{sj}^{\rm auto} + \sum_k A_{sk}^{\rm rad}} \ {\rm sec}^{-1}, \qquad (7)$$

so that Eq. (5) may be written as

$$S_s = (2.475\times 10^{-30})\frac{Q_s}{g_i E_{\rm res}} \ {\rm cm}^2\,{\rm eV}, \qquad (8)$$

where $E_{\rm res}$ is in eV.

Note that DR satellites are strongest when their upper levels have equal and large radiative and autoionization rates. Because most autoionization rates are all roughly the same (10^{12}–10^{14} sec^{-1}), S_s is primarily determined by the radiative rate. Radiative rates are not much affected by spectator electrons, so lines emitted from states with short lifetimes (large $A^{\rm rad}$), such as the electric dipole lines *w*, *y*, and *q*, have strong satellites, while line *z*, a magnetic dipole decay from the long-lived $^3S_1$ state, and line *x*, a magnetic quadrupole transition (blended with *y*), have essentially no satellites.

III. EXPERIMENT

A. EBIT, spectrometer, and data acquisition system

Neon $K\alpha$ spectra were collected on the Livermore EBIT [4] with a low-energy flat-crystal spectrometer [5]. The detector is a position-sensitive proportional counter and the spectrometer has a net resolving power of $\sim$500 when using a thallium acid phthalate (TAP) crystal. In this experiment, neutral neon atoms are continuously injected into the central trap region of EBIT where they are ionized and then electrostatically confined (radially) by a 70-μm-diam electron beam. A set of three electrodes provides longitudinal confinement. The nearly monoenergetic beam [$\sim$75 eV full width at half maximum (FWHM)] can be quickly raised and lowered, permitting study of the plasma while ionizing, recombining, or in equilibrium. For our experiment, the beam energy was ramped between 600 and 1200 eV with a 2.5-msec-period triangular wave form, reaching from the lowest DR resonances up to the He-like ionization threshold at 1196 eV. For every detected photon, the time and electron beam energy were recorded using the EBIT event-mode data acquisition system.

The period of the beam-energy sweep is comparable to the time scale for ionization of Li-like ions to the He-like state ($\sim$0.5 msec with an average electron beam density of 4×10^{12} cm^{-3}), but the ionization cross section (with thresholds of 239 eV for direct $2s$ ionization, and $\sim$900 eV for the various inner-shell excitation-autoionization channels) is constant to $\sim$8% over this energy range. Charge exchange with neutral neon atoms is the dominant recombination mechanism, with a time scale on the order of 10 msec. Radiative recombination of He-like ions occurs on a time scale of roughly 1 sec. *KLL* DR is much faster, but only occurs during the small fraction of time when the beam energy is on a resonance. Simulations show that the energy sweep is fast enough to keep the charge balance constant to better than 1%. Note that charge exchange recombination does not lead to any kind of $2\rightarrow 1$ emission here, since the recombined ions (Li-like and lower charge) are singly excited and cannot decay any lower than the $n=2$ level.

Once ionization equilibrium has been attained, following a periodic trap dump to remove higher-*Z* contaminants which build up over time, spectra are collected. Cross sections for excitation of the neon $K\alpha$ lines are of order 10^{-20} cm^2 near threshold, corresponding to time scales of approximately 10 msec. The typical time scale for radiative decay of excited ions is on the order of picoseconds (10^{-12} sec), so the chance of an excited ion undergoing further collisions before decaying is negligible. An exception is the highly forbidden transition from the $1s2s\ ^3S_1$ state that decays to produce line *z*; the radiative lifetime of that level is 91μ sec [1,2], which is slow enough compared to the electron energy slew rate to create the ''tail'' extending directly below *z*'s excitation threshold in Fig. 2, as well as permit collisional transfer to the $1s2p\ ^3P_{2,1}$ states that give rise to *x* and *y*, respectively. This, however, has no effect on our satellite line measurements.

Figure 2 is a plot of the spectral data, with wavelength along the horizontal axis and electron energy along the vertical. The He-like $K\alpha$ lines are prominent, with direct exci-

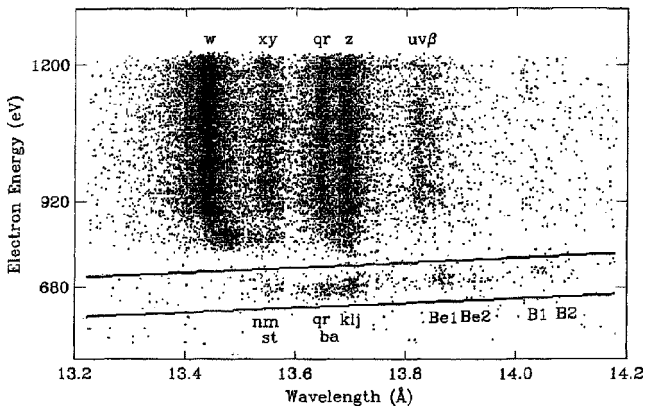

FIG. 2. Neon spectra, plotted versus wavelength and electron energy. Curved tails seen on several lines below the direct excitation threshold are from high-n DR satellites. The KLL spectrum contained within the angled box is shown in Fig. 3. Intensities of lines w and qr were summed from 920 to 1200 eV for normalization of Li-like and Be-like satellites.

tation thresholds for w, xy, and z of 922, 916, and 905 eV, respectively. The blend of q and r (the strongest Li-like satellites) is visible above its inner-shell collisional excitation threshold of 908 eV, and a fainter feature appears to the right of z. With roughly one-third the intensity of qr, this feature is the blend of Li-like u and v and the Be-like satellite β $(1s2s^2 2p\ ^1P_1 \rightarrow 1s^2 2s^2\ ^1S_0)$. Further to the right are faint B-like collisional satellites.

Below threshold are the DR satellites, the most prominent of which appear as curved tails on w and qr. (Recall that the straight tail below z is a radiative lifetime effect.) The KLM band ($n=3$ spectator electron) at the bottom of the tails (about 820 eV) is partially resolved while the KLL band ($n=2$) around 680 eV is quite distinct. The relatively strong KLL satellites below about 13.8 Å are Li-like satellites, while satellites with $\lambda > 13.8$ Å are Be-like. Some weak B-like KLL satellites can be seen beyond about 14 Å.

B. Intensity normalization method

Because the electron beam energy spread in EBIT ($\sim$75 eV FWHM) is so much wider than the intrinsic DR resonance widths, the intensity of a Li-like DR satellite line s emitted from EBIT is (ignoring presumably constant geometric factors such as the sizes and overlap of the electron beam and ion cloud)

$$I_s(E_{\rm av}) = v_e n_e n_{\rm He} S_s f(E_{\rm res} - E_{\rm av}), \tag{9}$$

where $E_{\rm av}$ is the average energy of the beam electrons and the function $f(E-E_{\rm av})$ describes the energy distribution of the electrons, which is approximately Gaussian. In our experiment, $n_{\rm He}$ is constant, and the electron beam current is held fixed so that $v_e n_e$ also can be assumed to be constant. If the energy distribution function is normalized so that

$$\int_{-\infty}^{\infty} f(E_{\rm res} - E_{\rm av}) dE = 1, \tag{10}$$

then integrating both sides of Eq. (9) over all energies (experimentally, by sweeping the beam energy up and down across a resonance) yields

$$I_s = v_e n_e n_{\rm He} S_s. \tag{11}$$

Because the intensity of Li-like satellites is proportional to the He-like ion density, their strengths must be normalized to some spectral feature whose intensity is also proportional to the He-like ion abundance. The best choice, since its theoretical cross section as a function of energy should be quite accurate, would be radiative recombination of He-like to Li-like ions, but the continuum photons produced by this process are too few to be observed. The next best choice is line w, the brightest line in the spectrum. Its emission processes are the best understood, and it has a smoothly varying cross section with only minor contributions from cascades and resonant excitation. Its intensity is given by

$$I_w(E_{\rm av}) = v_e n_e n_{\rm He} \sigma_w(E_{\rm av}). \tag{12}$$

Integrating over a range of energies, in this case from 920 to 1200 eV, then yields

$$I_w = v_e n_e n_{\rm He} \int_{920}^{1200} \sigma_w(E) dE. \tag{13}$$

When Eqs. (11) and (13) are divided, $v_e n_e n_{\rm He}$ cancels out, giving

$$S_s = \frac{I_s}{I_w} \int_{920}^{1200} \sigma_w(E) dE. \tag{14}$$

The resonance strengths of Be-like satellites are given by the same formula, but by normalizing to the collisionally excited Li-like qr blend instead of He-like w.

C. Polarization and spectrometer efficiency

The intensity of a line as observed by our spectrometer is equal to $I_l^{\rm obs} = G_l I_l$, where G_l, the spectrometer response function for line l, includes terms for spectrometer collecting area and efficiency, as well as the effects of polarization. Ion-electron collisions in EBIT are unidirectional, leading to unequal populations of magnetic sublevels, and so emission will in general be polarized and nonisotropic. Equation (14) then becomes

$$S_s = \frac{I_s^{\rm obs}}{G_s I_w^{\rm obs}} \int_{920}^{1200} G_w(E) \sigma_w(E) dE. \tag{15}$$

For unresolved satellites, G_s is an average for the blended lines, weighted by their theoretical resonance strengths.

To determine G for any line, we start with the equation for polarization, which is defined as

$$P = \frac{I_\parallel - I_\perp}{I_\parallel + I_\perp}, \tag{16}$$

where $I_\parallel$ is the intensity with polarization parallel to the electron beam direction and $I_\perp$ is for perpendicular polarization. The total intensity emitted toward the spectrometer, at 90° relative to the electron beam, is $I(90°)=I_\parallel+I_\perp$. The net observed intensity, after diffraction by a TAP crystal with reflectivities $R_\parallel$ and $R_\perp$, is then

$$I^{\rm obs}=A\,\eta(I_\parallel R_\parallel+I_\perp R_\perp), \tag{17}$$

where A is a geometrical term which includes the solid angle acceptance of the spectrometer and energy-independent variations in reflectivity across the crystal surface, and η is the quantum efficiency of the proportional counter detector, including the transmission of a thin window separating EBIT from the spectrometer. This can be rewritten, using the two preceding relations for P and $I(90°)$, as

$$I^{\rm obs}=A\,\eta I(90°)\,R_\parallel\left(\frac{1}{2}\right)\left[(1+P)+(1-P)\frac{R_\perp}{R_\parallel}\right]. \tag{18}$$

In order to relate the total line intensity integrated over all angles to that emitted toward the spectrometer, we use the equation [6]

$$I=\frac{3-P}{3}I(90°), \tag{19}$$

where P and $I(90°)$ are, respectively, the polarization and intensity of x rays emitted 90° to the electron beam. This relation applies for electric dipole transitions—which includes w, q, r, and all the other satellite lines under study—from ions excited by unidirectional electron collisions. Equation (18) can then be written as

$$I^{\rm obs}=\frac{3A\,\eta R_\parallel}{2(3-P)}\left[(1+P)+(1-P)\frac{R_\perp}{R_\parallel}\right]I=GI. \tag{20}$$

Apart from the polarization dependence, G is roughly the same for all the lines being studied. A was measured by scanning line w across the TAP crystal, and has a small linear rise at positions corresponding to longer wavelengths (5.3% higher at q than at w). $R_\parallel$ is constant with energy to within a fraction of 1%, but $R_\perp/R_\parallel$ gradually falls from 0.2444 for w to 0.2286 for q according to $\cos^{1.792}\theta_B$, as derived from theoretical calculations by Gullikson [7]. η also decreases slightly at longer wavelengths, by about 5.5% from w to q.

IV. ANALYSIS

Evaluation of resonance strengths using Eq. (15) requires a mix of experimental measurement ($I_s^{\rm obs}$ and $I_w^{\rm obs}$) and theoretical modeling (G_s, G_w, and σ_w). $I_s^{\rm obs}$ was measured for each DR satellite by collapsing the spectra contained in the angled extraction region shown in Fig. 2. The resulting spectrum is shown in Fig. 3. The integrated observed intensities of w and qr were found by summing all spectra above 920 eV and fitting each line or blend to determine the number of counts. Lorentzian profiles gave excellent fits to the above-threshold lines, and all linewidths were linked to the value obtained for w. The nm and st peaks, which blend together, were fit by setting their wavelength separation to 0.025 Å, the value predicted by Vainshtein and Safronova [8].

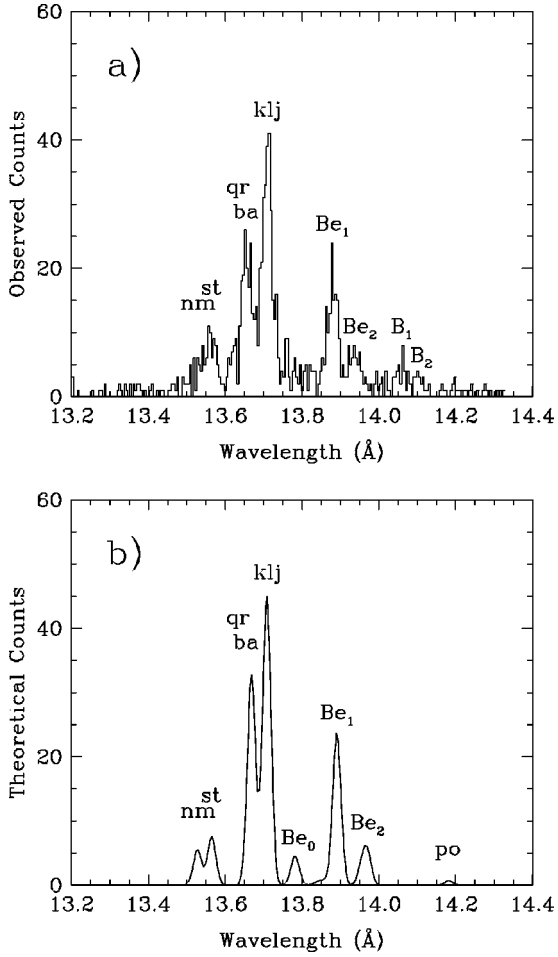

FIG. 3. Comparison of experimental and theoretical *KLL* spectra. Theoretical spectrum uses results from Chen [12,14,20], adjusted for spectrometer response.

The instrumental response factor G was evaluated for each DR satellite according to Eq. (20), with polarizations taken from Inal and Dubau [9] for the Li-like satellites and from Shlyaptseva *et al.* [10] for the Be-like, but modified to account for the fact that electron collisions in EBIT are not perfectly unidirectional because of a thermally induced transverse electron velocity component. As explained by Gu, Savin, and Beiersdorfer [11], the net (reduced) polarization for electric dipole transitions is given by

$$P=\mathcal{P}\frac{2-3\epsilon}{2-\epsilon\mathcal{P}}, \tag{21}$$

where ϵ is the ratio of the transverse energy component ($E_\perp$) and the total electron energy, and $\mathcal{P}$ is the polarization with zero transverse energy. We use the average of Chen's [12] and Karim and Bhalla's [13] predictions for the total (resonance) energies for each Li-like satellite, and Chen's [14] values for the Be-like lines. Estimates of $E_\perp$ on EBIT range

from 100 to 250 eV. Here we assume $E_\perp = 150$ eV, but as explained later, our results depend very little on the exact value.

To evaluate $\int G_w(E_{\rm av})\sigma_w(E_{\rm av})dE_{\rm av}$, we rely on theoretical calculations by Reed [15] of the collisional excitation cross sections for the $1s2p\ ^1P_1$ state and the $1s3s\ ^1S_0$ and $1s3d\ ^1D_2$ states which feed it by cascades with essentially 100% branching ratios. Cascades from corresponding higher-n levels were also included, with the assumptions that cross sections scale as $n^{-3.6}$ (by extension of Reed's results for $n=2$ and 3) and that branching ratios to $1s2p\ ^1P_1$ are still near 100%. Excitation to F, G, and higher terms is negligible, as is cascade feeding of the $1s2p\ ^1P_1$ state from triplet levels [16]. We find that $\int \sigma_w(E)dE$ from 920 to 1200 eV is 5.50×10^{-18} cm^2 eV, where we have extrapolated w's direct excitation cross section slightly below its 922-eV threshold to include the contributions of high-n DR, with cascades contributing just under 5% of the total. For comparison, the integrated cross section using the results of Sampson *et al.* [17] is 5.57×10^{-18} cm^2 eV, including cascades.

Reed [15] computed cross sections for each magnetic sublevel (m_J) to permit calculation of P_w, the polarization of w, following the formalism of Alder and Steffen [18], which is summarized by Gu, Savin, and Beiersdorfer [11] for application to EBIT. The resulting theoretical polarization of line w when excited by unidirectional electron collisions and viewed at 90° to the collision axis is 0.613 at threshold, with very little change up to 1200 eV. After including the effects of transverse electron velocity, the net polarization is reduced to about 0.49, depending only slightly on energy. The cross section and polarization results were then used to compute $G_w(E_{\rm av})$.

For the Be-like satellites, we normalize to $\int G_{qr}\sigma_{qr}dE$, using

$$G_{qr}\sigma_{qr} = G_q\sigma_q + G_r\sigma_r = G_q\sigma_{iq}W_q + G_r\sigma_{ir}W_r, \quad (22)$$

where σ_{iq} and σ_{ir} are the cross sections for excitation of the states that decay to produce q and r [see Eq. 3]. Lines q and r arise from identical configurations, with J values of 3/2 and 1/2, respectively. Since they are excited from the same Li-like ground state, on statistical grounds one would expect the ratio σ_{ir}/σ_{iq} to be 1/2. Using the results of Reed [15], which include excitation cross sections (by magnetic sublevel) for all 16 autoionizing Li-like Ne levels of the type $1s2l2l'$, we indeed find that σ_{ir}/σ_{iq} is very near 1/2 (0.493) for all energies. We also used those results to compute the polarization of q, which is 0.341 at threshold and $\sim$0.27 after depolarization. As will be discussed in Sec. V B, the actual values of W_q and W_r are not well known, but their ratio is, allowing us to accurately determine $G_{qr}(E)$.

To help understand the uncertainties involved in Eq. (15), one can rewrite it as

$$S_s = \frac{I_s^{\rm obs}}{I_w^{\rm obs}}\frac{G_s}{G_w}\int_{920}^{1200}\sigma_w(E)dE, \quad (23)$$

where G_w is the cross-section-weighted average of $G_w(E)$ [i.e., $\int G_w\sigma_w(E)dE/\int\sigma_w(E)dE$]. As seen from Eq. (20), when taking the ratio G_s/G_w, the $A\eta R_\parallel$ factors essentially cancel out, leaving only polarization-dependent terms. The intrinsic Li-like satellite polarizations are well known, as is the energy-dependent polarization of w, so the primary source of polarization uncertainty lies in the degree of depolarization, which is simply determined by $E_\perp$, according to Eq. (21). The G_s/G_w values listed in Table I were computed assuming that $E_\perp = 150$ eV, but using a different value has little effect. G_s/G_w varies by only about $\pm3\%$ for a 50-eV difference in $E_\perp$, except for the negatively polarized a and l lines, which are quite weak. The net uncertainty in G_s/G_w for blended lines is less than 1%.

Some of the Be-like satellites we observe are not listed by Shlyaptseva *et al.* [10], but we know the polarization of a few of them. The Be0 transition at 13.7806 Å (theoretical wavelength) involves an upper level with $L=0$, so its polarization is zero. The Be2 transition at 13.9566 Å has the same LSJ values as the Be1 transition at 13.8926, and so has the same polarization of $+0.439$. The six Be1 $^3P\rightarrow{}^3P$ transitions are between levels that are a mixture of S and D states, with the degree of polarization determined by how much of each component contributes to the levels involved. The strength of these lines is negligible, however, and we have simply assumed that $P=0$ in our calculations, as marked in Table II. We have also assumed $P=0$ for the Be1 line at 13.8887 Å. If the true polarization of that line were $+0.50\,(-0.50)$, then G_s/G_{qr} would be 40% larger (smaller), and the net measured strength of the Be1 blend would be 3% smaller (larger).

V. RESULTS AND COMPARISON WITH THEORY

Many theoretical papers on dielectronic recombination have been published, usually providing total recombination rates and summing over all n and l configurations. Although such results can be compared with laboratory measurements, most of the information about individual transitions and their rates is lost, and no line- or energy-specific comparisons with laboratory measurements can be made. A few authors, however, have published data with which we can make direct comparisons.

Vainshtein and Safronova (VS) [8] employed a perturbation technique on a basis of Coulomb functions using an expansion in powers of $1/Z$ to calculate radiative and Auger decay rates for all of the Li-like Ne $1s2s2l'$ satellites except g and h. It should be noted that they list $\tilde{q}$, which is misleadingly called a satellite intensity factor, but which uses only $A_{sf}^{\rm rad}$ instead of $\Sigma_k A_{sk}^{\rm rad}$ in the denominator of Eq. (7). For those pairs of satellite lines which share the same upper state—ab, cd, hi, kl, mn, op—we therefore determined the relevant radiative rates from their tables and computed the value of Q_s ourselves. Radiative decays other than those producing $n=2\rightarrow1$ satellites were not considered by VS. This is generally not important for the relatively strong lines we observed, but means that the strengths of some of the weaker satellites listed in Table I are overestimated.

Chen [12] carried out calculations for $1s2ln'l'$ levels with $n'=2$ and 3 (corresponding to KLL and KLM satel-

TABLE II. Theoretical atomic data for principal *KLL* dielectronic satellite transitions $1s2l^3 \rightarrow 1s^2 2l^2$ in Be-like Ne^{6+}. Polarizations are taken, when available, from Shlyaptseva *et al.* [10]. Theoretical values of λ and *S* are derived from results of Chen and Crasemann [20], with E_{res} taken from Chen [14]. Transitions are grouped to correspond with observed spectral features. Transition strengths are in units of 10^{-20} cm^2 eV.

Blend	Transition	E_{res} (eV)	*P*	G_s/G_{qr}	λ (Å)	*S*
Be0	$1s2s(^3S)2p^2\,^3S_1 \rightarrow 1s^2 2s2p\,^3P_0$	708.5	0	0.820	13.7806	0.18
	$1s2s(^3S)2p^2\,^3S_1 \rightarrow 1s^2 2s2p\,^3P_1$	708.5	0	0.820	13.7813	0.55
	$1s2s(^3S)2p^2\,^3S_1 \rightarrow 1s^2 2s2p\,^3P_2$	708.5	0	0.820	13.7831	0.96
Be1	$1s2p^3\,^3P_1 \rightarrow 1s^2 2p^2\,^3P_0$	727.4	0[a]	0.815[a]	13.8391	0.02
	$1s2p^3\,^3P_0 \rightarrow 1s^2 2p^2\,^3P_1$	727.4	0[a]	0.815[a]	13.8393	0.02
	$1s2p^3\,^3P_2 \rightarrow 1s^2 2p^2\,^3P_1$	727.4	0[a]	0.815[a]	13.8400	0.02
	$1s2p^3\,^3P_1 \rightarrow 1s^2 2p^2\,^3P_1$	727.4	0[a]	0.815[a]	13.8400	0.01
	$1s2p^3\,^3P_2 \rightarrow 1s^2 2p^2\,^3P_2$	727.4	0[a]	0.815[a]	13.8415	0.06
	$1s2p^3\,^3P_1 \rightarrow 1s^2 2p^2\,^3P_2$	727.4	0[a]	0.815[a]	13.8415	0.02
	$1s2s(^1S)2p^2\,^1S_0 \rightarrow 1s^2 2s^2\,^1P_1$	718.0	0	0.814	13.8593	0.24
	$1s2s(^3S)2p^2\,^3D_1 \rightarrow 1s^2 2s2p\,^3P_0$	701.5	0[a]	0.811[a]	13.8887	0.80
	$1s2s(^3S)2p^2\,^3D_1 \rightarrow 1s^2 2s2p\,^3P_1$	701.5	−0.429	0.607	13.8895	0.87
	$1s2s(^3S)2p^2\,^3D_2 \rightarrow 1s^2 2s2p\,^3P_1$	701.4	+0.333	1.014	13.8899	1.71
	$1s2s(^3S)2p^2\,^3D_2 \rightarrow 1s^2 2s2p\,^3P_2$	701.4	−0.429	0.607	13.8917	1.28
	$1s2s(^3S)2p^2\,^3D_3 \rightarrow 1s^2 2s2p\,^3P_2$	701.4	0.439	1.089	13.8926	4.14
Be2	$1s2p^3\,^3D_3 \rightarrow 1s^2 2p^2\,^3P_2$	704.0	+0.439	1.083	13.9566	1.00
	$1s2s(^1S)2p^2\,^1D_2 \rightarrow 1s^2 2s2p\,^1P_1$	710.8	+0.60	1.211	13.9704	1.75

[a]Polarizations unknown. *G* factors computed assuming $P=0$.

lites) with configuration interaction using the multiconfigurational Dirac-Fock method (MCDF). Results for the *m* and *n* satellites, which were not listed in that paper, were obtained by private communication, along with values of E_{res} for each line.

Nilsen [19] used relativistic MCDF bound states and distorted-wave Dirac continuum states in his calculations for $1s2ln'l' \rightarrow 1s^2 n''l''$ transitions, with $n',n''=2,3,4$. Karim and Bhalla (KB) [13] also studied *KLL*, *KLM*, and *KLN* DR, using intermediate coupling with a multiconfiguration Hartree-Fock-Slater atomic model, but only listed the radiative and Auger rates for selected transitions, omitting *a*, *b*, *q*, *r*, and several others. Wavelengths and rate data for all the lines were obtained by private communication [13].

The only published reference for Be-like DR rates is by Chen and Crasemann [20]. Although they list what they call ''*Q*'' values as well as wavelengths, those *Q*'s were calculated using A_{si}^{auto} rather than $\Sigma_j A_{aj}^{auto}$ in the denominator of Eq. (7). While the two are equivalent for Li-like $1s2l2l'$ levels, which can only autoionize to the single ground state of the He-like ion, Be-like $1s2l2l'2l''$ levels autoionize to create a Li-like ion which has three possible ground levels, namely $1s^2 2s\,^2S_{1/2}$, $1s^2 2p\,^2P_{1/2}$, and $1s^2 2p\,^2P_{3/2}$. For the purposes of the present comparison, Chen [20] provided the necessary Auger rates to let us compute the resonance strengths listed in Table II.

A. Wavelengths

Satellite wavelengths were determined by using *w*, *xy*, and *z* as reference lines with wavelengths of 13.4473, 13.5530, and 13.6990 Å, respectively, taken from Drake [21], where for λ_{xy} we have used the intensity-weighted average of λ_x and λ_y with $I_y/I_x=26$, as computed by Osterheld [16]. Drake's predictions for the corresponding He-like Al lines have been experimentally confirmed to approximately one part in 40 000 [22], so the above wavelengths are considered accurate to ±0.0003 Å. Results for the blended DR satellites are shown in Table III for Li-like lines and Table IV for Be-like lines. The wavelength of *qr* was also measured from the summed 920–1200 eV spectrum to be $\lambda = 13.6522 \pm 0.0005$ Å, but spectra from other EBIT measurements [1] with more counts indicate a wavelength of 13.6532 ± 0.0004 Å. The weighted average is 13.6528 ±0.0004 Å.

Although other collisionally excited lines are apparent in Fig. 2, their weakness, distance from lines of known wavelength, and blending make the determination of wavelengths rather problematic. Making generous allowance for uncertainties in extrapolating our wavelength scale, we find that the blend of Li-like *u* and *v*, along with some contribution from the Be-like β line, is at $\lambda = 13.839 \pm 0.004$ Å, and a B-like collisional satellite feature is at $\lambda = 14.041 \pm 0.005$ Å. The below-threshold features labeled as *B*1 and *B*2 are B-like *KLL* DR satellites, with wavelengths of 14.057 ±0.005 and 14.103 ± 0.007 Å, respectively.

As can be seen, the wavelength predictions of VS [8] are clearly superior to the others, with excellent self-consistency and agreement with our measurements. (We include separate results for *nm* and *st*, but those features are not well resolved from each other and the listed uncertainties, which are based purely on counting statistics, are too small. A more reliable result, for both wavelength and strength, is obtained from the

TABLE III. Comparison of measurement and theory for blended Li-like satellite lines. G_s/G_w is the net spectrometer response function for each blend (primarily dependent upon line polarization), normalized to the value for *w*. Experimental wavelengths were measured with respect to the He-like lines *w*, *xy*, and *z* using wavelengths from Drake [21]. Numbers in parentheses denote the uncertainty in the last digit(s). Wavelength differences are listed as $\Delta\lambda=\lambda_{\text{theory}}-\lambda_{\text{expt}}$, where λ_{theory} is the average for the blended lines, weighted by their theoretical as-observed intensities. Experimental resonance strengths were measured with respect to the integrated intensity of line *w* from 920 to 1200 eV, equal to 5.50×10^{-18} cm^2 eV according to theoretical cross sections calculated by Reed [15]. Listed uncertainties are statistical. $R=S_{\text{th}}/S_{\text{expt}}$ is the ratio of the theoretical and experimental resonance strengths for the blend. ''*KLL* sum'' refers to the sum of all observed *KLL* blends: *nm*, *st*, *qrba*, and *klj*. The wavelength of the *qr* blend, measured from data taken above its direct excitation threshold, is 13.6528 ± 0.0004 Å.

Blend	λ_{expt} (Å)	$\Delta\lambda^{a}$ (Å)	$\Delta\lambda^{b}$ (Å)	$\Delta\lambda^{c}$ (Å)	$\Delta\lambda^{d}$ (Å)	G_s/G_w	S_{expt}	R^{a}	R^{b}	R^{c}	R^{d}
nm	13.533(4)	0.005	−0.005	0.016	−0.012	0.639	1.08(22)	2.11	1.86	2.06	1.74
st	13.561(3)	0.003	0.005	0.019	−0.016	0.829	2.30(28)	0.72	0.92	0.76	0.83
nm+*st*	13.552(2)	−0.001	−0.002	0.013	−0.017	0.728	3.38(35)	1.17	1.22	1.18	1.12
qrba	13.655(2)	−0.001	0.014	0.022	0.001	0.802	6.45(51)	1.13	1.46	1.43	1.21
klj	13.7083(12)	0.001	0.001	0.025	−0.012	0.868	11.08(65)	1.33	1.10	1.31	1.15
KLL sum							20.91(96)	1.24	1.23	1.32	1.16

[a]Vainshtein and Safronova [8].
[b]Chen [12].
[c]Nilsen [19].
[d]Karim and Bhalla [13].

composite feature, *nm*+*st*.) VS also provide the best agreement with the *uvβ* blend at 13.839 Å; although, as noted above, this feature is difficult to interpret, we believe from examining higher-energy spectra that *β* lies slightly longward of *uv*, which is consistent with VS's prediction of $\lambda_{uv}=13.835$ Å. See Nilsen and Safronova [26] for a detailed comparison of wavelengths and radiative and autoionization rates predicted by Nilsen [19] and VS [8] and measured in other EBIT experiments.

B. Intensities

Theoretical resonance strengths for *KLL* lines were computed according to Eq. (8) using satellite intensity factors (Q_s's) from the theoretical papers listed above. Measured strengths were computed according to Eq. (15), where I_s^{obs} is the number of counts in the Li-like (Be-like) satellite and I_w^{obs} (I_{qr}^{obs}) is the number of counts in *w* (*qr*) in the 920–1200-eV summed spectrum. The general evaluation of $\int G_w\sigma_w dE$ and $\int G_{qr}\sigma_{qr}dE$ was described earlier; we now discuss the details of how $G_{qr}\sigma_{qr}$ was determined.

TABLE IV. Comparison of measurement and theory for blended Be-like satellite lines. G_s/G_{qr} is the net spectrometer response function for each blend, normalized to the value for the Li-like collisionally excited satellite blend *qr*. Experimental resonance strengths were measured with respect to the integrated intensity of *qr*, using theoretical excitation cross sections calculated by Reed [15] and integrated from 920 to 1200 eV (which yields $\int\sigma_{iq}=3.04\times10^{-18}$ cm^2 eV) and fluorescence yields of $W_q=0.680$ and $W_r=0.595$. Listed uncertainties in experimental wavelengths and strengths are statistical.

Key	G_s/G_{qr}	λ_{th} (Å)	λ_{expt} (Å)	S_{th}	S_{expt}
Be0	0.820	13.782		1.69	~1
Be1	0.926	13.890	13.879±0.003	9.19	9.50±0.72
Be2	1.064	13.966	13.941±0.004	2.75	2.29±0.35

We use Reed's [15] predictions for σ_{iq} and σ_{ir} [see Eq. (22)]. The integral of σ_{iq} from 920 to 1200 eV is 3.04×10^{-18} cm^2 eV, and 0.493 times that for *r*, but we also need to know the fluorescence yields for those two lines. VS, Chen, and Nilsen all agree that $W_r/W_q=0.875$ to within one-half percent, while KB predict a slightly higher value of 0.909. We have adopted 0.875 for our calculations. There was much greater disagreement on the value of W_q, however, with predictions of 0.351 (Chen), 0.519 (Nilsen), 0.524 (KB), and 0.637 (VS). From a measurement of the ratio $\sigma_{z\text{ISI}}/\sigma_{qr}$ [23], where $\sigma_{z\text{ISI}}$ is the cross section for production of line *z* via inner-shell ionization of Li-like Ne (which, for direct ionization, leaves the He-like ion in a $1s2s\,^3S_1$ state 3/4 of the time), and using Reed's [15] *q* and *r* excitation cross sections and Younger's [24] direct inner-shell ionization cross section, we derive $W_q=0.68$, a value higher than any of the theoretical predictions, although the VS value is not too different. Using Lotz's [25] formula for the ionization cross section yields essentially the same value ($W_q=0.65$), and we have used 0.68 in our calculations.

The resulting theoretical resonance strengths are presented in Tables III and IV. Individual results for *nm* and *st* are somewhat suspect because of blending, but their composite strength should be reliable. For comparison with the observed spectrum, we used Chen's predictions [12,14] to predict what the spectrum would look like after accounting for polarization and instrumental effects (see Fig. 3), assuming an ion abundance ratio of $n_{\text{Li}}/n_{\text{He}}=0.10$.

Reasonably good agreement is found between theory and experiment for the Li-like blends, although total theoretical resonance strengths range from 16% to 32% (average 23%) higher than measured values. Variations are larger for the

three individual blends, and range from 10% to 46% higher than measured values. In particular, the predictions of Chen and Nilsen seem quite high for q and r, and Nilsen and VS have notably greater strengths for j and k. Statistical uncertainties (1σ) for the measured strengths range from 10% (for $nm+st$) to 5% (for the total of all Li-like KLL lines).

In addition to statistical uncertainties in the observed spectra, there are several possible sources of systematic experimental error. Uncertainties related to polarization and relative spectrometer efficiency are at the 1% level, and so the primary sources of error are likely to be in the measured and theoretical integrated intensity of w, and in our assumption of constant $v_e n_e n_{\rm ion}$ [see Eqs. (11) and (12)].

The estimated uncertainty in the electron beam energy is $\sim\pm 10$ eV. When summing spectra over a range of 280 eV, from 920 to 1200 eV, this corresponds to $\sim 5\%$ uncertainty in the number of integrated counts. Uncertainty in the theoretical cross section for w is difficult to estimate, but believed to be of order 10%. Our measured satellite resonance strengths are directly proportional to $\int \sigma_w$, so if a value more reliable than 5.50×10^{-18} cm^2 eV becomes available, our results can be easily scaled.

Variations in the value of $v_e n_e n_{\rm ion}$ arise from changes in trap conditions, particularly the He-like/Li-like ion ratio and the beam-ion overlap, as the electron beam sweeps up and down over a factor of 2 in energy. As mentioned before, simulations of time-dependent charge balance show that the energy sweep was fast enough to keep the charge balance constant at the 1% level. Since beam current was held fixed for this measurement, electron density increased as electrons moved more slowly at lower energies. This would tend to increase the beam-ion overlap as the electron space charge attracted ions more strongly. The result of this extra attraction, however, would be more trapped ions at low energies, thus increasing the apparent satellite intensities and the disagreement between theory and measurement if this effect were taken into account. Beiersdorfer *et al.* [27] estimated the increase at between 5% and 20% in their measurement of resonance strengths for He-like Fe, but at the very low energies required to study neon, beam instabilities are expected to counteract some or all of this increase, and we make no net adjustment for these effects in our analysis.

We do, however, conservatively increase our net systematic error to $\pm 15\%$, apart from uncertainties in σ_w. Given that statistical and line-fitting uncertainties are between 5% and 10%, and that theoretical predictions of Li-like satellite resonance strengths are between 10% and 46% higher than measured values (and on average 23% higher), our results suggest that existing models overpredict KLL DR rates.

Our measurements agree best (a 16% overall difference) with the predictions of KB. In the only other published measurement of He-like neon DR, which used what we assume is essentially the same atomic modeling code as KB, Ali *et al.* [28] reported results from an electron beam ion source (which counts ions, rather than x rays) and compared the predicted and measured total (non-line-specific) KLL (and $KLM+$) DR cross sections onto He-like neon. They obtained good agreement, although systematic errors were not well understood, and all relevant recombination channels may not have been included in the model.

For the Be-like KLL blends, experimental and theoretical strengths agree to within roughly the statistical uncertainty of the measurement. Systematic uncertainties are similar to those for the Li-like lines. The potentially largest error lies in our normalization to the theoretical value of σ_q, which depends on the excitation cross section for the upper level and the fluorescence yield. As noted earlier, theoretical values of W_q range from 0.35 to 0.64, and we believe the actual value is close to 0.68. Given such large disparities, it is rather surprising that the theoretical Li-like satellite resonance strengths agree with each other as well as they do.

VI. CONCLUSIONS

We have described an experimental measurement of the strengths and wavelengths of the KLL dielectronic recombination satellites in Li-like and Be-like neon. We find that existing theoretical calculations for Li-like satellites predict strengths that are marginally too large, and that the wavelength predictions of Vainshtein and Safronova [8] are by far the most accurate, agreeing with our measurements to within the experimental uncertainty, which was as good as one part in 30 000. The single set of theoretical calculations for Be-like satellites agrees well with our measured resonance strengths, although the intensity normalization method highlights significant uncertainty over the fluorescence yield for the Li-like satellite line q; existing predictions for that yield vary by nearly a factor of 2, and only one is close to what we measure.

ACKNOWLEDGMENTS

We would like to thank M. Chen, K. Reed, and A. Osterheld for their atomic modeling calculations, K. Karim for providing an extended version of previously published calculations, R. Ali for a reprint of his EBIS measurements, and D. Nelson and E. Magee for their technical support. This work was performed under the auspices of the U.S. Department of Energy by the Univeristy of California, Lawrence Livermore National Laboratory under Contract No. W-7405-ENG-48 and was supported by the NASA Space Astrophysics Research and Analysis Program.

[1] B.J. Wargelin, P. Beiersdorfer, and S.M. Kahn, Phys. Rev. Lett. **71**, 2196 (1993).

[2] E. Träbert, P. Beiersdorfer, G.V. Brown, A.J. Smith, S.B. Utter, M.F. Gu, and D.W. Savin, Phys. Rev. A **60**, 2034 (1999).

[3] A.H. Gabriel, Mon. Not. R. Astron. Soc. **160**, 99 (1972).

[4] M.A. Levine, R.E. Marrs, J.R. Henderson, D.A. Knapp, and M.B. Schneider, Phys. Scr. **T22**, 157 (1988).

[5] P. Beiersdorfer and B.J. Wargelin, Rev. Sci. Instrum. **65**, 13

(1994).
[6] I.C. Percival and M.J. Seaton, Philos. Trans. R. Soc. London, Ser. A **251**, 113 (1958).
[7] E. Gullikson (private communication).
[8] L.A. Vainshtein and U.I. Safronova, At. Data Nucl. Data Tables **21**, 49 (1978).
[9] M.K. Inal and J. Dubau, J. Phys. B **22**, 3329 (1989).
[10] A.S. Shlyaptseva, R.C. Mancini, P. Neill, P. Beiersdorfer, J.R. Crespo López-Urrutia, and K. Widmann, Phys. Rev. A **57**, 888 (1998).
[11] M.F. Gu, D.W. Savin, and P. Beiersdorfer, J. Phys. B **32**, 5371 (1999).
[12] M.H. Chen, At. Data Nucl. Data Tables **34**, 301 (1986); rates for *m* and *n* and resonance energies for all lines (private communication).
[13] K.R. Karim and C.P. Bhalla, J. Quant. Spectrosc. Radiat. Transf. **51**, 557 (1994); K. R. Karim—wavelengths, resonance energies, and rates for individual lines (private communication).
[14] M.H. Chen, Phys. Rev. A **31**, 1449 (1985); additional resonance energies (private communication).
[15] K. Reed (private communication).
[16] A.L. Osterheld (private communication).
[17] D.H. Sampson, S.J. Goett, and R.E.H. Clark, At. Data Nucl. Data Tables **29**, 467 (1983).
[18] K. Alder and R.M. Steffen, in *The Electromagnetic Interaction in Nuclear Spectroscopy*, edited by W.D. Hamilton (American Elsevier, New York, 1975), Chap. 1, pp. 1–38; R. M. Steffen and K. Alder, *ibid.*, Chap. 12, pp. 505–582.
[19] J. Nilsen, At. Data Nucl. Data Tables **38**, 339 (1988).
[20] M.H. Chen and B. Crasemann, At. Data Nucl. Data Tables **37**, 420 (1987); M.H. Chen—additional Auger rates (private communication).
[21] G.W.F. Drake, Can. J. Phys. **66**, 586 (1988).
[22] B.J. Wargelin, P. Beiersdorfer, D.A. Liedahl, S.M. Kahn, and S. von Goeler, Astrophys. J. **496**, 1031 (1998).
[23] B.J. Wargelin, Ph.D. thesis, University of California, Berkeley, 1993.
[24] S.M. Younger, J. Quant. Spectrosc. Radiat. Transf. **26**, 329 (1981).
[25] W. Lotz, Z. Phys. **202**, 205 (1967).
[26] J. Nilsen and U.I. Safronova, J. Quant. Spectrosc. Radiat. Transf. **49**, 371 (1993).
[27] P. Beiersdorfer *et al.*, Phys. Rev. A **46**, 3812 (1992).
[28] R. Ali, C.P. Bhalla, C.L. Cocke, M. Schulz, and M. Stöckli, in *Recombination of Atomic Ions*, edited by W.G. Graham *et al.* (Plenum Press, New York, 1992), p. 193.